


Real-Time Observation of Poly(3-alkylthiophene) Crystallization and Correlation with Transient Optoelectronic Properties

Bryan W. Boudouris,^{†,§} Victor Ho,^{†,§} Leslie H. Jimison,[‡] Michael F. Toney,[‡] Alberto Salles,[‡] and Rachel A. Segalman^{*,†}

[†]Department of Chemical and Biomolecular Engineering, University of California, Berkeley, and Materials Science Division, Lawrence Berkeley National Laboratory, Berkeley, California 94720, United States

[‡]Department of Materials Science and Engineering, Stanford University, Stanford, California 94305, United States

[‡]Stanford Synchrotron Radiation Lightsource, Menlo Park, California 94025, United States

 Supporting Information

INTRODUCTION

Conjugated polymers, with inherently rigid molecular backbones, have attracted much attention due to their relatively favorable charge transport properties, high optical absorption coefficients, and ease of processing from common organic solvents.^{1–3} However, these materials form a semicrystalline film upon solution-casting that is far removed from the equilibrium microstructure; therefore, the processing history of the active layer in an electronic device greatly influences the morphology, which in turn affects performance.^{4–8} The degree of crystallinity is a particularly crucial factor in obtaining high-performance organic thin film devices.^{9–11} Usually in thin film polymeric semiconductors, the charge mobility in the amorphous regions is significantly lower than that in the crystalline domains.^{12–15} As such, studying the degree of crystallinity in semiconducting polymer thin films and developing polymers and processing conditions that control the fraction of amorphous polymer is of great interest. In general, previous experimental studies have varied the degree of crystallinity in semiconducting polymer thin films by varying deposition conditions, solvent vapor pressures, solid-state processing, and postprocessing conditions (e.g., annealing treatments) to kinetically trap films at various points during crystallization.^{12,16–19} However, these methods allow only limited control, making it difficult to form completely amorphous films or to dictate the crystalline fraction in order to generate a series of specimens with a continuum in the polymer percent crystallinity. Furthermore, nonideal film-to-film reproducibility hinders an easy interpretation of these experiments. As a result, determining how semicrystalline polymer films crystallize, and the effect of this sequence on observable optoelectronic properties has proven extremely difficult. Because this fundamental understanding is lacking, the synthesis of each new polymer requires the reformulation of a new set of processing conditions in order to maximize device performance.²⁰ As such, the practical limits of these materials are unknown, and optimization of polymer-based electronics is largely Edisonian and significantly time intensive.

Poly(3-alkylthiophenes) (P3ATs), specifically, have risen to the fore of the organic electronics community over the past 15 years due to their useful optical and electronic properties.^{21–24} In fact, poly(3-hexylthiophene) (P3HT) has become the standard p-type material in polymer-based organic field-effect transistors

(OFETs)^{25,26} and the standard electron-donating material in bulk heterojunction organic photovoltaic (OPV) devices.^{18,27,28} Usually these active layers are deposited from solution at room temperature, which is significantly removed from the crystallization temperature of P3HT ($T_c \sim 180$ °C).^{29,30} This large degree of undercooling leads to kinetically trapped microstructures, and the morphology is difficult to control.^{31–33} On the other hand, we have shown recently that poly(3-(2'-ethyl)hexylthiophene)^{34–36} (P3EHT, chemical structure inset in Figure 2) has comparable optoelectronic properties to that of P3HT and poly(3-dodecylthiophene) (P3DDT) and that its melting and liquid crystal transition temperatures are much lower ($T < 120$ °C).³⁷ This makes P3EHT an ideal candidate for understanding the impact of crystallization on optoelectronic properties for a technologically important class of semiconducting polymers, poly(3-alkylthiophenes), especially as interest in solid-state processing of organic electronic materials is increasing.^{38,39}

Here, we correlate the physics of semicrystalline ordering of a P3EHT ($M_n \sim 10.8$ kg/mol, PDI ~ 1.2) thin film to the polymer's optoelectronic properties utilizing *in situ* measurements on an experimentally convenient time scale when quenching from the melt to room temperature. Specifically, we demonstrate that while the polymer crystallinity continually increases over time, the field-effect transistor (FET) hole mobilities abruptly increase 60-fold at a threshold time. We attribute this mobility onset to the formation of a thin film crystalline network in an amorphous matrix. Furthermore, we show that the evolution of ultraviolet–visible (UV–vis) absorption and photoluminescence (PL) profiles in the thin film correlate well with the polymer crystallization. The polymer solidification process is readily observed as the crystal structure of the P3EHT thin film is monitored as a function of time after quenching to room temperature (from the melted ($T_m \approx 80$ °C) state) with grazing-incidence X-ray diffraction (GI-XRD). The appearance of higher order reflections in the GI-XRD spectra with time after quenching indicates three-dimensional crystallization occurring over the course of ~ 1 h. These real-time observations of crucial structure–transport relationships of this model macromolecular semiconductor

Received: June 10, 2011

Revised: July 14, 2011

Published: August 03, 2011

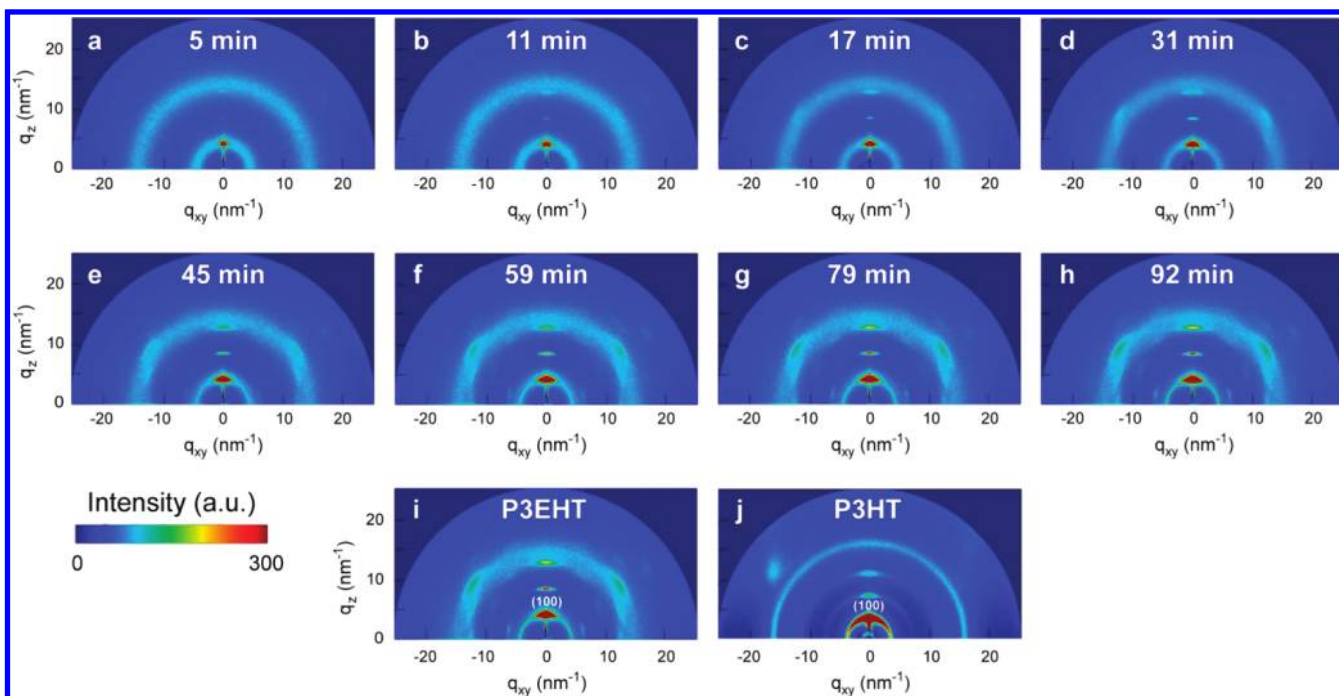


Figure 1. Grazing-incidence X-ray diffraction (GI-XRD) patterns of a P3EHT thin film at (a) 5, (b) 11, (c) 17, (d) 31, (e) 45, (f) 59, (g) 79, and (h) 92 min after quenching to room temperature from the isotropic melt. Comparison of patterns for (i) P3EHT 92 min after quenching to room temperature and (j) P3HT with the (100) reflection labeled. The color scale for (j) is 0–600 au due to a longer exposure time for the P3HT thin film.

provide insight into how polythiophene ordering influences hole transport and optical absorption, which, in turn, should lead to design rules for semiconducting polymer architectures, the opportunity for solid-state processing of semiconducting polymer thin films, and better control of the final active layer microstructures in polymer-based organic electronics.

RESULTS AND DISCUSSION

Thin films of P3EHT are crystallographically highly oriented (strong crystalline texture) relative to other P3ATs, as evidenced by greater resolution of reflections in grazing-incidence X-ray diffraction (GI-XRD) patterns and pole figures (Figure S5). This allows for determination of a potential triclinic unit cell for P3EHT ($a \approx 0.73$ nm, $b \approx 1.03$ nm, $c \approx 1.54$ nm, $\alpha \approx 72^\circ$, $\beta \approx 98^\circ$, and γ was assumed to be 90°), which is qualitatively different from that of the cells proposed for other P3ATs.^{32,40,41} From the GI-XRD pattern of P3EHT (Figure 1i), the (100), (200), and (300) reflections are observed along the vertical axis at $q = 4.38$, 8.62 , and 12.9 nm⁻¹, respectively; this preferential alignment relative to the substrate is seen in the P3HT film as well (Figure 1j). However, unlike other P3ATs, the (011) line of reflections is located at $q_{xy} = 6.15$ nm⁻¹ (e.g., the (010) can be seen at $q_{xy} = 6.15$ nm⁻¹ and $q_z = 2.0$ nm⁻¹). This indicates that P3EHT does not occupy an orthorhombic unit cell. While the complete molecular packing determination are beyond the scope of this paper, the position of the (010) reflection leads to lattice parameter of $b = 1.03$ nm (see Figure S1b for complete peak assignments). While this unit cell description results in an intermolecular distance very similar to P3HT, an exact determination of the π – π stacking distance between first and second P3EHT chains in the unit cell is precluded without a complete P3EHT crystal structure.

In addition to the improved crystalline texture, the lower thermal transitions of P3EHT relative to other P3ATs allows crystallization to be monitored *in situ* and correlated to changes in optoelectronic properties, which are also measured as a function of crystallization time. GI-XRD patterns of the P3EHT thin films collected after quenching from the isotropic melt to room temperature reveal the progression of crystallization as a function of time. Shortly after quenching (Figure 1a), the diffraction pattern is similar to that of the polymer film in the melt (Figure S1) with an amorphous halo being the dominating feature. A weak peak exists along the vertical near 4.50 nm⁻¹, corresponding to the expected repeat distance of ~ 1.4 nm along the sample normal (nominally the alkyl stacking direction) according to powder diffraction of bulk P3HT and P3EHT, and is indexed as the (100) Bragg reflection.³⁷ After 10 min, two additional orders of (h00) peaks are visible, and the intensity of the (h00) peaks continues to increase with time (labeled in Figure 1i). Approximately 31 min after quenching, a number of off-axis peaks appear, including the (010), corresponding to the π – π stacking repeat. With further increasing time, the amorphous halo decreases in intensity, and the (h00), (010), and off-axis peaks become more defined, but without significant increases in intensity.

A 60-fold increase in the field-effect hole mobility occurred over the course of polymer crystallization after quenching from the melt (*vide infra*) and can be explained by the crystallization of the P3EHT film. Specifically, the relative degree of P3EHT crystallinity is determined quantitatively as a function of time by measuring approximate pole figures of the (100) reflection (Figure S2).^{42,43} The measured crystallinity steadily increases over ~ 75 min after quenching before reaching a constant value (Figure 2). Because of the geometry of grazing-incidence diffraction, these approximate pole figures (Figure S2b) do not probe

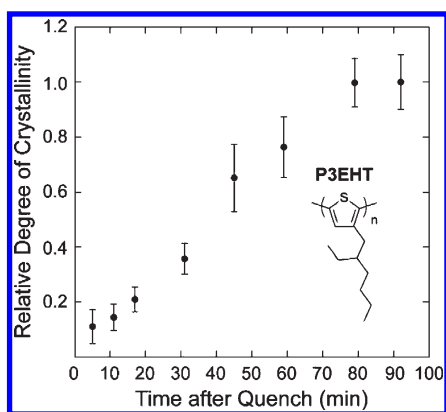


Figure 2. Relative degree of crystallinity (rDoC) as a function of time for the P3EHT thin film, based on intensity of the (100) Bragg reflection. Here, all rDoC values are normalized such that the final time ($t = 93$ min) has a value of 1.0. The chemical structure of P3EHT is the inset.

crystallites with their (100) direction oriented within a few degrees of the substrate normal; this requires local specular scans. However, in our case, the approximate pole figures are quite accurate (see Supporting Information). The relative degree of crystallinity (rDoC) was calculated from the approximate pole figures according to eq 1.

$$\text{rDoC} \propto \int_{\chi_{\min}}^{\pi/2} \sin(\chi) I(\chi) d\chi \quad (1)$$

where χ_{\min} is the minimum χ allowed by the GI-XRD geometry. The film with the highest degree of crystallinity in this data set, corresponding to the longest time after quench, was assigned a value of 1.0, against which other thin films were compared.

In addition to the increased intensity of peaks in GI-XRD, thin film UV–vis absorption and photoluminescence (PL) profiles show a clear red-shift, a signature of increased conjugation length in organic semiconductors,⁴⁴ with time after quenching from the melt. When the isotropic melt is quenched directly to room temperature, the absorption profile is initially broad and features only one maximum at $\lambda = 463$ nm (Figure 3a).⁴⁵ This absorbance profile is akin to a dilute solution of a regioregular P3AT in a good solvent⁴⁶ and the absorbance profile of a regiorandom P3AT thin film.^{47,48} In both of these, the P3AT lacks semicrystalline order and no interchain optoelectronic coupling exists. This comparison shows that the P3EHT film is noncrystalline immediately after quenching to room temperature, consistent with the GI-XRD profile. However, at a rDoC value as low as 0.15 (10 min after quenching), the profile begins to red-shift and a vibronic shoulder appears at a higher wavelength ($\lambda \approx 573$ nm), indicating the formation of small crystalline regions. As the time after quench approaches 1 h, the P3EHT absorption coefficient increases and reaches a relatively high value in agreement with previous reports.^{46,49} This thin film absorption behavior of P3EHT is in stark contrast to that of a P3HT thin film quenched to room temperature from the melt.⁵⁰ In the P3HT case, the absorption profile remains constant over the course of 1 h (Figure S3); this is consistent with rapid crystallization of the straight-chain alkyl-substituted P3AT at room temperature due to significant undercooling.

Furthermore, the absorption profiles show an isosbestic point is present at $\lambda = 452$ nm during the course of crystallization. This

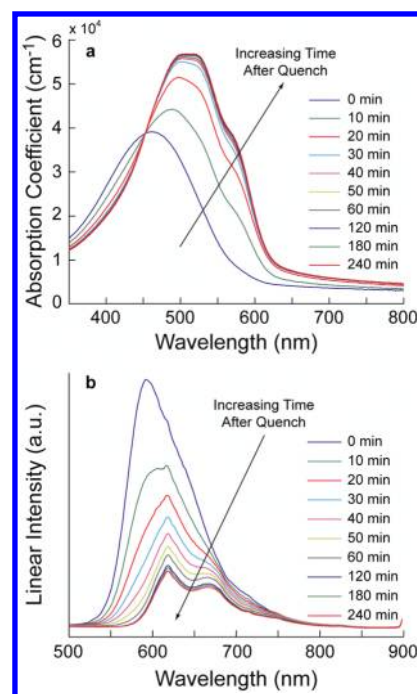


Figure 3. (a) Time-resolved thin film UV–vis light absorption spectra of P3EHT during crystallization. Thin films were heated to the isotropic melt ($T = 120$ °C) under vacuum and then quenched to room temperature to obtain an amorphous morphology which exhibits an absorption profile similar to that of a dilute P3EHT solution. A red-shift in the absorption profile is observed over the course of crystallization, and the presence of a low-energy vibronic shoulder is observed also. The isosbestic point at $\lambda = 452$ nm is consistent with a nondegradation event that shows the transition from one absorbing species to another. (b) Real time, steady-state photoluminescence (PL) emission spectra of a P3EHT thin film during crystallization. Thin films were heated to the isotropic melt ($T = 120$ °C) under vacuum and then quenched to room temperature. A red-shift in the emission profile is observed over the course of crystallization, and a secondary, lower energy emission peak emerges. The excitation wavelength was chosen as the isosbestic point to ensure a constant absorption value. Final film thicknesses were ~ 60 nm as estimated by profilometry.

indicates that only two species contribute to the overall absorption profile and that the total absorption profile is a linear combination of each component's absorption spectrum.^{51,52} These two absorbing species are taken to be the amorphous domains, where the absorption occurs without interchain coupling, and crystalline domains, in which correlations between neighboring chains increase the P3EHT conjugation length. This increase in conjugation length decreases the bandgap and shifts the absorption profile of the crystalline domains to longer wavelengths.²⁵ Thus, the decrease in absorption intensity at shorter wavelengths ($\lambda < 452$ nm) and the increase in absorption intensity at longer wavelengths ($\lambda > 452$ nm) can be recognized as a signature of the conversion of amorphous to semicrystalline polymer domains with time.

Thin film photoluminescence (PL) data collected in real time (Figure 3b) further demonstrate the formation of interchain P3EHT aggregates over ~ 1 h after quenching from the isotropic melt. Immediately after quenching, the PL data resemble that of an amorphous P3AT thin film⁵³ or a dilute P3AT solution with a broad peak at $\lambda < 600$ nm.^{54,55} As early as 10 min, a clear red-shift in the maximum of the emission profile to $\lambda = 617$ nm is observed

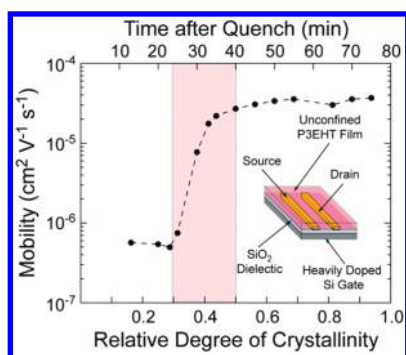


Figure 4. Field-effect hole mobility (μ_h) as a function of the relative degree of crystallinity as determined from the data in Figure 2 (the upper axis shows the time after quenching from the melt). The inset schematically depicts the silicon oxide-gated bottom gate, bottom contact field-effect transistor (FET) device geometry. A bottom contact geometry ensures that the polymer is not confined by an electrode interface during microstructural organization. Mobility values were calculated in the saturation regime ($V_D = -60$ V).

and a small shoulder at lower energy ($\lambda = 665$ nm) emerges. This difference of ~ 0.18 eV commonly is interpreted as the energetic difference associated with the phonon energy of the C=C symmetric stretch of the conjugated backbone.⁵⁴ With time, there is an increase in the emission at $\lambda = 665$ nm and a decrease in emission at $\lambda = 617$ nm. Previous efforts have shown that the lower wavelength peak is associated with amorphous regions of a P3AT film while the higher wavelength peak is representative of emission from a crystalline region of the film.³³ Furthermore, it has been demonstrated that the increase of the lower energy emission peak relative to the higher energy emission is consistent with an increase in polythiophene conjugation length.^{48,54} In fact, the decrease in emission at $\lambda = 617$ nm has been seen for P3AT thin films with increasing regioregularity.⁵⁶ Therefore, we conclude that the semicrystalline order in our films leads to decreased PL emission at $\lambda = 617$ nm. Additionally, these PL data and the P3EHT thin film absorption data confirm that the optical properties are intrinsically coupled with the microstructure of the P3AT and that we can observe these structure–property evolutions in real time.

In contrast to the relatively uniform increase in the rDoC and absorption coefficient as a function of time, there is a much sharper increase in the mobility (Figure 4). The first measurement made after quenching ($t = 12$ min) shows a P3EHT hole mobility (μ_h) of $\mu_h \sim 6 \times 10^{-7} \text{ cm}^2 \text{ V}^{-1} \text{ s}^{-1}$, which is low and consistent with an amorphous scattering pattern observed in the GI-XRD spectrum at this point after quenching to room temperature. This low mobility persists up to $\text{rDoC} \approx 0.30$ ($t \approx 28$ min), at which time a dramatic increase (Figure 4, shaded region) in hole mobility of ~ 60 -fold occurs, which suggests the formation of a semicrystalline network that is better suited for carrying charge. Note that this is also the point where the π – π stacking reflections and other off-axis peaks appear in the GI-XRD spectrum. Finally, the hole mobility saturates at $\mu_h \sim 4 \times 10^{-5} \text{ cm}^2 \text{ V}^{-1} \text{ s}^{-1}$ for $\text{rDoC} \approx 0.5$, remains relatively constant over the remainder of the experiment, and is nearly of the same order as for low molecular weight P3DDT and P3EHT polymers.³⁷ This asymptotic value of the hole mobility is ~ 10 -fold less than that previously observed for a similar molecular weight P3HT spun-coat from chloroform.⁵⁷ Because our previous work has shown that P3DDT and P3EHT have similar FET hole

mobilities under similar deposition conditions,³⁷ the lowered hole mobility in the FET device shown here relative to previous work is ascribed to the nonoptimized P3EHT FET fabrication conditions (e.g., the lack of a surface modification at the organic–dielectric interface) and the quick quench to room temperature employed. Despite very high crystalline texture in P3EHT as evidenced by the GI-XRD spectra, these device preparation conditions could result in a large number of disorder-associated transport barriers across the macroscopic channel, which would hinder the absolute value of the hole mobility measured. Furthermore, we speculate that the difference in unit cell between P3EHT and P3HT could also contribute to the lowered mobility in P3EHT relative to P3HT. Importantly, however, these data allow for the better understanding of how increases in crystallinity affects charge transport due to the ease of processing associated with P3EHT. For instance, at higher rDoC (>0.5) the hole mobility saturates despite a 2-fold increase in the relative rDoC. Once a series of semicrystalline domains that can be crossed easily are available for charge transport, holes readily move along these high mobility pathways.

In addition to having a much longer crystallization time than straight-chain poly(3-alkylthiophenes) at room temperature, the final P3EHT diffraction pattern (achieved after ~ 90 min, Figure 1f) displays more off-axis peaks than a P3HT film (Figure 1g) and has more highly oriented crystalline texture. The presence of significant off-axis peaks implies coherent three-dimensional molecular packing, which is the case for well-ordered films of other liquid crystalline polymers such as poly-(5,5-bis(3-dodecyl-2-thienyl)-2,2-bithiophene) (PQT)⁵⁸ or poly-(2,5-bis(3-alkylthiophen-2-yl)thieno[3,2-*b*]thiophene) (pBTTT).⁵⁹ Both of these materials possess a lower density of side chains compared to P3HT, allowing for molecular interdigitation.⁶⁰ The side-chain complexity in the P3EHT structure may result in a similar interdigitation effect. Furthermore, the broader peak in the pole figure for a P3HT film of comparable thickness indicates significantly more oriented crystalline texture in the P3EHT film (Figure S5). This texture is independent of quenching time, as shown by the similar shapes of the approximate pole figures (Figure S2c). The crystallites are well-oriented with the ($h00$) vector normal to the substrate (Figure S2b), which suggests that on average there is smaller spread in out-of-plane orientations between neighboring crystallites. In other systems, polymer films with long-range crystallographic alignment have been used to make high-performance field-effect transistors.^{9,61} Therefore, P3EHT may prove to be a material whose microstructure can be manipulated easily for the fabrication of high-performance organic electronic devices as well as a useful material for the real-time study of P3AT crystallization and optoelectronic studies.

CONCLUSIONS

Because it has readily accessible melting and liquid crystalline transitions, poly(3-(2'-ethyl)hexylthiophene) was used as a model polymer to study the time-resolved crystallization of poly(3-alkylthiophenes), an important class of semiconducting polymers. Because of the slow crystallization of P3EHT when quenched from the melt to room temperature, we observe the formation of a semicrystalline thin film with a strongly preferred crystallographic orientation over the course of ~ 1 h, and we are able to correlate this microstructural ordering in the film directly with changes in the optoelectronic properties of the polymer. Specifically, a P3EHT thin film shows a clear transition in hole

mobility that we interpret as the formation of a percolating crystalline network; at this point (rDoC increasing from 0.3 to 0.5), the hole mobility increases 60 times relative to the amorphous film. Furthermore, the optical properties of the polymers shift from a regime of amorphous-like behavior where there are only intramolecular correlations to that of a crystalline P3AT where intermolecular interactions play crucial roles at the same point that FET hole mobility sharply increases. By utilizing a P3AT that crystallizes on an experimental convenient time scale at room temperature, we can correlate how the degree of crystallinity in P3AT thin films affect the material's optical and electronic properties in real time. The better understanding of these crucial relationships, in turn, can help guide the design of new semiconducting polymers and the new active layer processing conditions in organic electronic devices.

■ ASSOCIATED CONTENT

S Supporting Information. Detailed experimental techniques, additional grazing-incidence X-ray diffraction (GI-XRD) data, poly(3-hexylthiophene) (P3HT) UV-vis data, and raw field-effect transistor (FET) data. This material is available free of charge via the Internet at <http://pubs.acs.org>.

■ AUTHOR INFORMATION

Corresponding Author

*E-mail: segalman@berkeley.edu.

Author Contributions

^SAuthors contributed equally.

■ ACKNOWLEDGMENT

R.A.S., V.H., and B.W.B. gratefully acknowledge support through the DOE-Office of Science Plastic Electronics Program at Lawrence Berkeley National Laboratories, supported via the Director, Office of Science, Office of Basic Energy Sciences (BES), Division of Materials Sciences and Engineering, of the US Department of Energy (DOE) under Contract DE-AC02-05CH11231. Device fabrication and characterization were performed at the Molecular Foundry, a Lawrence Berkeley National Laboratory user facility supported by the Office of Science, BES, DOE. Portions of this research were carried out at the Stanford Synchrotron Radiation Lightsource, a Directorate of SLAC National Accelerator Laboratory and an Office of Science User Facility operated for the U.S. Department of Energy Office of Science by Stanford University. V.H. gratefully acknowledges the National Science Foundation for a graduate fellowship. L.H.J. acknowledges support from Toshiba Corporation through the Center for Integrated Systems at Stanford. A.S. gratefully acknowledges support from the National Science Foundation in the form of a CAREER Award. R.A.S. acknowledges support from the Alfred P. Sloan Foundation.

■ REFERENCES

- (1) *Handbook of Conducting Polymers*; Skotheim, T. A., Elsenbaumer, R. L., Reynolds, J. R., Eds.; Marcel Dekker: New York, 1998; Vol. 2.
- (2) Loo, Y. L.; McCulloch, I. *MRS Bull.* **2008**, *33*, 653–662.
- (3) Shaheen, S. E.; Ginley, D. S.; Jabbour, G. E. *MRS Bull.* **2005**, *30*, 10–19.
- (4) Tsao, H. N.; Mullen, K. *Chem. Soc. Rev.* **2010**, *39*, 2372–2386.

- (5) Inigo, A. R.; Tan, C. H.; Fann, W.; Huang, Y. S.; Perng, G. Y.; Chen, S. A. *Adv. Mater.* **2001**, *13*, 504–508.
- (6) Huang, Y. F.; Inigo, A.; Chang, C. C.; Li, K. C.; Liang, C. F.; Chang, C. W.; Lim, T. S.; Chen, S. H.; White, J.; Jeng, U. S.; Su, A. C.; Huang, Y. S.; Peng, K. Y.; Chen, S. A.; Pai, W. W.; Lin, C. H.; Tameev, A.; Novikov, S.; Vannikov, A.; Fann, W. S. *Adv. Funct. Mater.* **2007**, *17*, 2902–2910.
- (7) Salleo, A.; Kline, R. J.; DeLongchamp, D. M.; Chabinyc, M. L. *Adv. Mater.* **2010**, *22*, 3812–3838.
- (8) Jimison, L. H.; Salleo, A.; Chabinyc, M. L.; Bernstein, D. P.; Toney, M. F. *Phys. Rev. B* **2008**, *78*, 125319.
- (9) McCulloch, I.; Heeney, M.; Bailey, C.; Genevicius, K.; Macdonald, I.; Shkunov, M.; Sparrowe, D.; Tierney, S.; Wagner, R.; Zhang, W. M.; Chabinyc, M. L.; Kline, R. J.; McGehee, M. D.; Toney, M. F. *Nature Mater.* **2006**, *5*, 328–333.
- (10) Zhang, R.; Li, B.; Iovu, M. C.; Jeffries-EL, M.; Sauve, G.; Cooper, J.; Jia, S. J.; Tristram-Nagle, S.; Smilgies, D. M.; Lambeth, D. N.; McCullough, R. D.; Kowalewski, T. *J. Am. Chem. Soc.* **2006**, *128*, 3480–3481.
- (11) Lunt, R. R.; Benziger, J. B.; Forrest, S. R. *Adv. Mater.* **2010**, *22*, 1233–1236.
- (12) Yang, H.; Shin, T. J.; Yang, L.; Cho, K.; Ryu, C. Y.; Bao, Z. *Adv. Funct. Mater.* **2005**, *15*, 671–676.
- (13) Masubuchi, S.; Kazama, S. *Synth. Met.* **1995**, *74*, 151–158.
- (14) Sirringhaus, H.; Brown, P. J.; Friend, R. H.; Nielsen, M. M.; Bechgaard, K.; Langeveld-Voss, B. M. W.; Spiering, A. J. H.; Janssen, R. A. J.; Meijer, E. W.; Herwig, P.; de Leeuw, D. M. *Nature* **1999**, *401*, 685–688.
- (15) Sirringhaus, H.; Brown, P. J.; Friend, R. H.; Nielsen, M. M.; Bechgaard, K.; Langeveld-Voss, B. M. W.; Spiering, A. J. H.; Janssen, R. A. J.; Meijer, E. W. *Synth. Met.* **2000**, *111*, 129–132.
- (16) Erb, T.; Zhokhavets, U.; Gobsch, G.; Raleva, S.; Stuhn, B.; Schilinsky, P.; Waldauf, C.; Brabec, C. J. *Adv. Funct. Mater.* **2005**, *15*, 1193–1196.
- (17) Clarke, T. M.; Ballantyne, A. M.; Nelson, J.; Bradley, D. D. C.; Durrant, J. R. *Adv. Funct. Mater.* **2008**, *18*, 4029–4035.
- (18) Li, G.; Shrotriya, V.; Huang, J. S.; Yao, Y.; Moriarty, T.; Emery, K.; Yang, Y. *Nature Mater.* **2005**, *4*, 864–868.
- (19) Chang, J.-F.; Sun, B.; Breiby, D. W.; Nielsen, M. M.; Sölling, T. I.; Giles, M.; McCulloch, I.; Sirringhaus, H. *Chem. Mater.* **2004**, *16*, 4772–4776.
- (20) Chabinyc, M. L.; Jimison, L. H.; Rivnay, J.; Salleo, A. *MRS Bull.* **2008**, *33*, 683–689.
- (21) McCullough, R. D. *Adv. Mater.* **1998**, *10*, 93–116.
- (22) Osaka, I.; McCullough, R. D. *Acc. Chem. Res.* **2008**, *41*, 1202–1214.
- (23) Thompson, B. C.; Fréchet, J. M. J. *Angew. Chem., Int. Ed.* **2008**, *47*, 58–77.
- (24) Peet, J.; Heeger, A. J.; Bazan, G. C. *Acc. Chem. Res.* **2009**, *42*, 1700–1708.
- (25) Sirringhaus, H.; Brown, P. J.; Friend, R. H.; Nielsen, M. M.; Bechgaard, K.; Langeveld-Voss, B. M. W.; Spiering, A. J. H.; Janssen, R. A. J.; Meijer, E. W.; Herwig, P.; de Leeuw, D. M. *Nature* **1999**, *401*, 685–688.
- (26) Wang, G. M.; Swensen, J.; Moses, D.; Heeger, A. J. *J. Appl. Phys.* **2003**, *93*, 6137–6141.
- (27) Padinger, F.; Rittberger, R. S.; Sariciftci, N. S. *Adv. Funct. Mater.* **2003**, *13*, 85–88.
- (28) Ma, W. L.; Yang, C. Y.; Gong, X.; Lee, K.; Heeger, A. J. *Adv. Funct. Mater.* **2005**, *15*, 1617–1622.
- (29) Kuila, B. K.; Nandi, A. K. *J. Phys. Chem. B* **2006**, *110*, 1621–1631.
- (30) Verploegen, E.; Mondal, R.; Bettinger, C. J.; Sok, S.; Toney, M. F.; Bao, Z. A. *Adv. Funct. Mater.* **2010**, *20*, 3519–3529.
- (31) Jimison, L. H.; Toney, M. F.; McCulloch, I.; Heeney, M.; Salleo, A. *Adv. Mater.* **2009**, *21*, 1568–1572.
- (32) Kayunkid, N.; Uttiya, S.; Brinkmann, M. *Macromolecules* **2010**, *43*, 4961–4967.

- (33) Brinkmann, M.; Chandezon, F.; Pansu, R. B.; Julien-Rabant, C. *Adv. Funct. Mater.* **2009**, *19*, 2759–2766.
- (34) Andersson, M. R.; Thomas, O.; Mammo, W.; Svensson, M.; Theander, M.; Inganas, O. *J. Mater. Chem.* **1999**, *9*, 1933–1940.
- (35) Zhang, Y.; Tajima, K.; Hashimoto, K. *Macromolecules* **2009**, *42*, 7008–7015.
- (36) Zhang, Y.; Tajima, K.; Hirota, K.; Hashimoto, K. *J. Am. Chem. Soc.* **2008**, *130*, 7812–7813.
- (37) Ho, V.; Boudouris, B. W.; Segalman, R. A. *Macromolecules* **2010**, *43*, 7895–7899.
- (38) Baklar, M. A.; Koch, F.; Kumar, A.; Domingo, E. B.; Campoy-Quiles, M.; Feldman, K.; Yu, L. Y.; Wobkenberg, P.; Ball, J.; Wilson, R. M.; McCulloch, I.; Kreouzis, T.; Heeney, M.; Anthopoulos, T.; Smith, P.; Stingelin, N. *Adv. Mater.* **2010**, *22*, 3942–3947.
- (39) Muller, C.; Zhigadlo, N. D.; Kumar, A.; Baklar, M. A.; Karpinski, J.; Smith, P.; Kreouzis, T.; Stingelin, N. *Macromolecules* **2011**, *44*, 1221–1225.
- (40) Prosa, T. J.; Winokur, M. J.; Moulton, J.; Smith, P.; Heeger, A. J. *Macromolecules* **1992**, *25*, 4364–4372.
- (41) Brinkmann, M.; Wittmann, J.-C. *Adv. Mater.* **2006**, *18*, 860–863.
- (42) See Supporting Information for detailed data analysis.
- (43) Baker, J. L.; Jimison, L. H.; Mannsfeld, S.; Volkman, S.; Yin, S.; Subramanian, V.; Salleo, A.; Alivisatos, A. P.; Toney, M. F. *Langmuir* **2010**, *26*, 9146–9151.
- (44) Winokur, M. J.; Slinker, J.; Huber, D. L. *Phys. Rev. B* **2003**, *67*, 184106.
- (45) Note that the sample is annealed in a vacuum oven at $T = 120$ °C for at least 30 min, which ensures the removal of any residual solvent from the spin-coating procedure used to generate the thin film.
- (46) Boudouris, B. W.; Molins, F.; Blank, D. A.; Frisbie, C. D.; Hillmyer, M. A. *Macromolecules* **2009**, *42*, 4118–4126.
- (47) Chen, T. A.; Wu, X. M.; Rieke, R. D. *J. Am. Chem. Soc.* **1995**, *117*, 233–244.
- (48) Brown, P. J.; Thomas, D. S.; Kohler, A.; Wilson, J. S.; Kim, J. S.; Ramsdale, C. M.; Sirringhaus, H.; Friend, R. H. *Phys. Rev. B* **2003**, *67*, 064203.
- (49) Thompson, B. C.; Kim, B. J.; Kavulak, D. F.; Sivula, K.; Mauldin, C.; Fréchet, J. M. J. *Macromolecules* **2007**, *40*, 7425–7428.
- (50) P3HT films were quenched from 230 °C to room temperature. Because of P3HT's high melting transition, the isotropic phase could not be accessed prior to degradation.
- (51) Kankare, J.; Lukkari, J.; Pajunen, T.; Ahonen, J.; Visy, C. *J. Electroanal. Chem.* **1990**, *294*, 59–72.
- (52) Vinokurov, I. A.; Kankare, J. *J. Phys. Chem. B* **1998**, *102*, 1136–1140.
- (53) Ruseckas, A.; Namdas, E. B.; Ganguly, T.; Theander, M.; Svensson, M.; Andersson, M. R.; Inganas, O.; Sundstrom, V. *J. Phys. Chem. B* **2001**, *105*, 7624–7631.
- (54) Clark, J.; Silva, C.; Friend, R. H.; Spano, F. C. *Phys. Rev. Lett.* **2007**, *98*, 125319.
- (55) Cook, S.; Furube, A.; Katoh, R. *Energy Environ. Sci.* **2008**, *1*, 294–299.
- (56) Bai, X.; Holdcroft, S. *Macromolecules* **1993**, *26*, 4457–4460.
- (57) Kline, R. J.; McGehee, M. D.; Kadnikova, E. N.; Liu, J.; Fréchet, J. M. J.; Toney, M. F. *Macromolecules* **2005**, *38*, 3312–3319.
- (58) Jimison, L. H.; Salleo, A.; Chabinyc, M. L.; Bernstein, D. P.; Toney, M. F. *Phys. Rev. B* **2008**, *78*, 125319.
- (59) Chabinyc, M. L.; Toney, M. F.; Kline, R. J.; McCulloch, I.; Heeney, M. *J. Am. Chem. Soc.* **2007**, *129*, 3226–3237.
- (60) Kline, R. J.; DeLongchamp, D. M.; Fischer, D. A.; Lin, E. K.; Richter, L. J.; Chabinyc, M. L.; Toney, M. F.; Heeney, M.; McCulloch, I. *Macromolecules* **2007**, *40*, 7960–7965.
- (61) Hamadani, B. H.; Gundlach, D. J.; McCulloch, I.; Heeney, M. *Appl. Phys. Lett.* **2007**, *91*, 243512.